Nexo Revista Científica
Vol. 36, No. 06, pp. 1087-1102/Diciembre 2023

ISSN-E 1995-9516
Universidad Nacional de Ingeniería
http://revistas.uni.edu.ni/index.php/Nexo
https://doi.org/10.5377/nexo.v36i06.17466

Synthesis and characterization of ZNO: CU and AG bimetallics nanoparticles by sol gel method

Síntesis y caracterización de nanopartículas bimetálicas de ZNO: CU y AG por método sol gel

H. Amer Mohammed*, M. Jasim Mohammed, H. Ammar Ayesh

Department of Physics,College of Science, Diyala University, Diyala Governorate, Iraq

amerm0296@gmail.com

(recibido/received: 17-agosto-2023; aceptado/accepted: 15-noviembre-2023)

ABSTRACT

Different weight ratios of Cu-silver-doped and non-doped ZnO nanoparticles were created, By using XRD, FTIR, UV-visible spectroscopy, FESEM, and EDS the presence of nanoparticles in the sol-gel (ZnO) and (ZnO: Ag and Cu) techniques was confirmed, the JCPDS standard card for Zn (01-080-0074) validated the hexagonal ZnO structure by X-ray diffraction for (ZnO) and (ZnO:Ag and Cu). we calculated the average crystal size of all the produced samples, and we observe that the crystal size grows as the ratio of copper and silver doping rises. According to the FTIR data, O-H expansion is responsible for the expected distinctive absorption band in the vicinity of (3090-3665 cm). Because KBr quickly absorbs CO, it is possible that the peaks in the range (1550-1630 cm) are caused by the KBr utilized. These peaks are related to the stretching vibrations of C=O that are symmetric and asymmetric. The stretching vibration of the ZnO bond can be seen in the form of a prominent peak in the (350–780 cm) range. When Ag and Cu are entered to the doped ZnO samples, the peak strength declines, indicating the start of Ag and Cu clusters on the surface of ZnO nanoparticles. The bond position was shifted as a result of alteration in bond length brought about by the substitution of Ag+ ions at the ZnO lattice sites. According to the UV-VIS measurements, pure ZnO has a peak at 370 nm that becomes red at 569 nm. With increasing concentrations of Ag and Cu, the nanocomposites show high absorption in the visible region because the peaks shift monotonously to longer wavelengths and cause the energy gap value to decrease by 3, 2.958, 2.76, 2.74, 2.69, and 2.5 eV, respectively. According to the FESEM data from IMAGE J, the nanoparticles have a spherical or nearly spherical form. Zn, Ag, and Cu elements may be seen in the EDS data.

Keywords: Cu-Ag doped ZnO; Sol-gel; Bimetallic; Nanoparticals

RESUMEN

Se crearon diferentes proporciones de peso de nanopartículas de ZnO dopadas y no dopadas con Cu-plata. Mediante el uso de XRD, FTIR, espectroscopía UV-visible, FESEM y EDS se determinó la presencia de nanopartículas en el sol-gel (ZnO) y (ZnO:Ag). y Cu), la tarjeta estándar JCPDS para Zn (01-080-0074) validó la estructura hexagonal del ZnO mediante difracción de rayos X para (ZnO) y (ZnO:Ag y Cu). Calculamos el tamaño promedio de los cristales de todas las muestras producidas y observamos que el tamaño del cristal crece a medida que aumenta la proporción de dopaje de cobre y

plata. Según los datos FTIR, la expansión O-H es responsable de la banda de absorción distintiva esperada en las proximidades de (3090-3665 cm-). Debido a que el KBr absorbe rápidamente CO, es posible que los picos en el rango (1550-1630 cm-1) sean causados por el KBr utilizado. Estos picos están relacionados con las vibraciones de estiramiento de C=O que son simétricas y asimétricas. La vibración de estiramiento del enlace ZnO se puede observar en forma de un pico prominente en el rango (350-780 cm). Cuando se introducen Ag y Cu en las muestras de ZnO dopadas, la fuerza máxima disminuye, lo que indica el inicio de grupos de Ag y Cu en la superficie de las nanopartículas de ZnO. La posición del enlace se desplazó como resultado de la alteración en la longitud del enlace provocada por la sustitución de iones Ag+ en los sitios de la red de ZnO. Según las mediciones UV-VIS, el ZnO puro tiene un pico a 370 nm que se vuelve rojo a 569 nm. Con concentraciones crecientes de Ag y Cu, los nanocompuestos muestran una alta absorción en la región visible porque los picos cambian monótonamente a longitude de onda más largas y hacen que el valor de la brecha de energía disminuya en 3, 2,958, 2,76, 2,74, 2,69 y 2,5 eV, respectivamente. Según los datos de la FESEM de IMAGE J, las nanopartículas tienen forma esférica o casi esférica. En los datos del EDS se pueden ver elementos Zn, Ag y Cu.

Palabras claves: ZnO dopado con Cu-Ag; sol-gel; Bimetálico; Nanopartículas

1. INTRODUCTION

Because of their prominent properties that are advantageous for catalysis, researchers are now concentrating on the production of metal nanoparticles, nanostructures, and nanomaterials (M.A. Meyers et al.,2006), Compound such as polymer preparations (M. Seyedi et al.,2015), disease diagnosis and treatment (Ado J.et al.,2008), sensing technology (Lin Q.et al.,2004- Vo-Dinh. A.,2004), and recording optoelectronic media labeling (M.T. Swihart.,2003). The intended qualities of the material have a direct impact on the mounting technique selection. Chemical techniques are the most common ones used by researchers worldwide for experimental conditions since they directly affect the desired qualities of a composite material. Depending on its gravity, a material becomes a composite. Conductors and semiconductors are continually sought-after materials because we live in an advanced technological and electrical age. (K. A. Abdullah et al.,2017- A. Kołodziejczak-Radzimska et al.,2014). It is known that adding metal ions to some materials might improve their semiconductor characteristics (A. Kołodziejczak et al.,2014). Pure zinc oxide is an element of zinc that occurs naturally as a white solid that turns orange when heated as a result of distortions in the lattice. It is a non-toxic, insoluble in water semiconductor with the molecular symbol ZnO. In mineral acids, it dissolves. In laboratories, zinc oxide is chemically prepared by burning the metal in the air or heating its carbonates or nitrates. It is distinguished by having a high value for electrical conductivity, The infrared area of the spectrum reflects in the visible region of the spectrum which has a high transmittance. Cm.22.65 belongs to the (negative) type (Galstyan, V.et al.,2015). In the form of the mineral zincite, zinc oxide is present in the earth's crust, however the majority of the zinc oxide The energy gap of commercially available, synthetically produced TCO, which is expected to be 3.37 eV wide, makes it an equally significant transparent semiconductor material. At ambient temperature, the exciton binding energy is also substantial (60 me) (P. UIKEY et al.,2016). Zinc oxide is used for producing ultraviolet light, as a varistor, in piezoelectric converters, as an air-flow sensor, on the surface of things that resemble acoustic waves, and in many other electrical devices since it possesses all these qualities (M. H. Huang et al.,2001). Furthermore, zinc oxide is a common element in medicinal and cosmetic goods due to its non-toxic, antibacterial, and UV radiation protective qualities (K. O. Siegel et al.,2013). Monometallic nanoparticles have received less attention in science and technology than bimetallic ones, which are composed of two distinct metals. The metals that make up bimetallic nanoparticles and their nanoscale size determine how they behave. These are created by fusing different metallic nanoparticle architectural structures. They really have a propensity to maximize the energy of the metallic combinations'

absorption band, giving us a flexible biosensing tool. These features, which might include size-dependent optical, electrical, thermal, and catalytic impacts, may be different from those of pure elemental particles (Z. Medynska et al.,2013).

2. MATERIAL AND METHODS

2.1. material

Sol-gel self-combustion was used to create the nanomaterials. Zinc nitrate, silver nitrate, copper nitrate, citric acid, and ammonia solution were the raw materials employed in this technique. The raw materials, their level of purity, and their resource are displayed at table 1.

Table 1. Chemical composition for raw materials used.

compounds	Chemical formula	Purity%	Molecular weight (g/mole)	Supplier
Zinc Nitrate	$Zn(NO_3)_2.6H_2O$	99	297.49	CDH
Silver Nitrate	$AgNO_3$	99	169.87	Alpha chemika
Copper (II) Nitrate	$Cu(NO_3)_2.3H_2O$	99	241.60	CDH
Ammonia solution	NH_4OH	98	35.05	Alpha chemika
Citric Acid	$C_6H_8O_7.H_2O$	99	210.14	Alpha chemika

2.2. Synthesis of ZnO and ZnO: Cu and Ag nanoparticles

1. For preparing pure ZnO and ZnO:Ag and Cu nanoparticles, raw materials of "Zinc nitrate ($Zn(NO_3)_2.6H2O$), silver nitrate ($AgNO_3$) , copper nitrate ($Cu(NO_3)_2.3H2O$) were weighed according to the weight ratios as shown in Table 2 . In desired proportion, the raw materials dissolved in 150 ml of DI water and stirred at 500 rpm for 30 minutes until gel clear solutions.
2. 7.8802 g of Citric acid ($C_6H_8O_7.H_2O$) was dissolved in 100 ml of DI water and mixed for 30 minutes at 500 rpm to gel clear solution.
3. Under stirring at 500 rpm, 100 ml of citric' acid solution with the final ratio (1:2 Citric acid: Zinc nitrate) has been added carefully and slowly as reduction agent to the 150 ml of (zinc, copper, and silver nitrates) solution, and the final volume of mixtures solution was 250 ml. the molarity of Zinc nitrate was 0.3 M in final volume of solution. After this step, the solution was homogenized
4. The "ammonia (NH_4OH)" solution was distilled to the total mixture solution to obtain pH = 4
5. Then the solution is left by continuous magnetic stirring (rpm 500) at a temperature of 75°C inside the solution for 3-4 hours until obtained a viscose gel
6. The final product (gel) was oven-dried at 100 °C for 5 hours. doped and non-doped nanoparticles were obtained
7. The dried gel was calcined for 3 hours at a temperature of 500 degrees Celsius to obtain highly crystalline "Zinc oxide and silver and copper-doped zinc oxide" nanoparticles
8. The calcined nanoparticles were crushed with high quality mortar to get fine powders.
9. The steps 1 to 8 were repeated six times.

Table 2. Weight ratios of the prepared samples.

Sample	Zn%	Ag%	Cu%	W=Zn	W=Ag	W=Cu	W=Citric Acid
Z1	100	0	0	22.31175	0	0	7.88025
Z2	95	2.5	2.5	21.19616	0.312956	0.738435	
Z3	90	5	5	20.08058	0.625913	1.47687	
Z4	85	7.5	7.5	18.96499	0.938869	2.215305	
Z5	80	10	10	17.8494	1.251825	2.95374	
Z6	75	12.5	12.5	13.38705	1.564781	3.692175	

Citric Acid ($C_6H_8O_7.H_2O$)	$Zn(NO_3)_2.6H_2O$	AgNO3	$Cu(NO_3)3H_2O$
MW	MW (Zn)	MW (Ag)	MW (Cu)
210.14	297.49	169.87	241.6

3. RESULTS AND DISCUSSION

3.1 Structural Properties

3.1.1 X-Ray Diffraction Results

XRD analysis was performed to determine the exact crystal structure, and crystalline size of the Nano composites. The XRD patterns of the as prepared Nano composites (Z1, Z2, Z3, Z4, Z5 and Z6) as shown in figure 1, reveal well-defined diffraction peaks at 31.73°, 34.38°, 36.22°, 47.48°, 56.54° and 62.77° Indexed as (100), (002), (101), (102), (110), (103) quartzite hexagonal planes of the ZnO phase, in agreement with JCPDS Card No. ZnO (01-076-0704) (G. Muruganantham et al.,2012). However, the powders (Z2, Z3, Z4, Z5 and Z6) reveal the appearance of peaks for CuO at 35.55°, 38.05°, 38.67°, 47.95°, 57.98°, 62.01°, 32.14°, 45.63° and 75.01° belonging to (-111), (111), (200), (-202), (-113), (110), (-112), and (-222) having mono crystal structure according to the standard JCPDS Card No. (01-080-0076) (Gnanaprakasam A et al.,2016). which increases its intensity decreases with decreasing full width at half maximum and increasing doping rate. (Z2, Z3, Z4, Z5 and Z6) produces deflection peaks at 62.81°, 64.30°, 65.6°,29.80°,54.54°,56.01°,65.63°and 54.60° associated with (220), (022), (110), (202), (310), (-402) and (222) level. Return to its monoclinic conforming to the standard card JCPDS Card No. AgO (01-074-1743) (V. Vaiano et al.,2018). The calculation of the distance from the crystalline levels in undoped and doped ZnO is using Bracks law in diffraction

$$n\lambda = 2d_{hkl} \sin\theta \qquad \ldots\ldots\ldots \qquad (1)$$

n: is an integer number, called the order of reflection, λ: is the X-ray wavelength, d_{hkl}: is the spacing between atomic planes in the crystalline phase, θ: is the Bragg angle of the diffracted beam. yielding a result that aligns with the data provided in the international card. The prevailing trend was adopted, and it is preferred to know the changes in the properties of the ZnO crystal structure. From the relation of Scherer's Formula, the crystallite size was calculated by increasing the concentration of Ag, the position of the peak is shifted towards lower values, as shown in Table. This shift indicates a partial replacement of Ag+ ions in the ZnO lattice and an increase in the lattice a and c scales, as expected (Karunakaran,

C. et al.,2011). This subject pertains to the examination of the ionic size density among Ag+ ions (0.126 nanometer) as well as Zn+2 ions (0.074 nm) within the ZnO lattice, specifically focusing on the overlapping of Ag ions., which slows down the crystallization of the host as a result of the formation of oxygen voids due to the difference in the ionic diameter between them. This makes a decrease in the crystal size. As for an increase in the concentration of Cu, it did not have a significant effect on the host, Zn, because the ionic diameters of both are very close, since the ionic diameter is Cu+2 (0.073) nm. Moreover, there was no substantial alteration in the depiction of the summits. The phenomenon of diffraction is observed when a separation of Ag ions occurs within the lattice structure of ZnO, hence preventing their replacement for ZnO sites (F. Sun et al.,2012- Samavati, A. et al.,2016). The presence from AgO and CuO phases, shown by the minor shift in the peak positions of the ZnO phase, provides evidence for the successful production of ZnO nanocomposites. The observed decreased crystal size Table 2, as determined by the application of the Scherrer equation:

$$D=k\,\lambda/\,\beta\cos\theta \quad \ldots \quad (2)$$

exhibits a considerable decrease upon the introduction of copper and silver doping, which aligns with findings published in a prior investigation (K. Ravichandran et al.,2016). For all the prepared nanoparticles, the values of the formation factor (Tc) were calculated using the relationship:

$$TC=\frac{I(hkl)}{I0(hkl)}\frac{1}{n}\sum_{i=1}^{n}\frac{I(hkl)}{I0(hkl)} \quad \ldots \quad (3)$$

which describes the dominant and preferred direction (hkl) for crystal growth as shown in Table (3), and the results showed that the values of the formation factor for all models were greater than one. (Tc > 1) for the prevailing trend of (101) (002) (112) level. From this result, it is clear to us that there is no stable trend for a specific granular growth, and there was no significant explanation for the growth of both directions together, and we noticed that there is a decrease in the formation factor values with an increase in the doping rates, and there was no change in the prevailing trend, as shown in Figure 3. The micro-strain (ε) and the dislocations density (δ) were calculated depending on the relationships respectively for all of the results shown in Table the micro-strain (ε) with dislocation intensity (δ) were determined using equations:

$$\varepsilon = \beta\cos\theta/4 \quad \ldots \quad (4)$$

$$\delta = \frac{1}{D^2} \quad \ldots \quad (5)$$

respectively, for all the data presented in Table 3. The present study revealed that the incorporation of silver (Ag) and copper (Cu) dopants into zinc oxide (ZnO) resulted in a notable augmentation in both micro-strain and dislocation intensity. However, as the doping level increased, a subsequent decline in these parameters was seen. This phenomenon can be attributed to the ordered arrangement of atoms within the crystal lattice. As for the fifth sample, the density of dislocations and micro-strain increases, and this indicates an irregularity in the arrangement of atoms when crystallizing in the fifth sample. Figure 5, shows the relationship between micro-strain, dislocation density, and crystalline size.

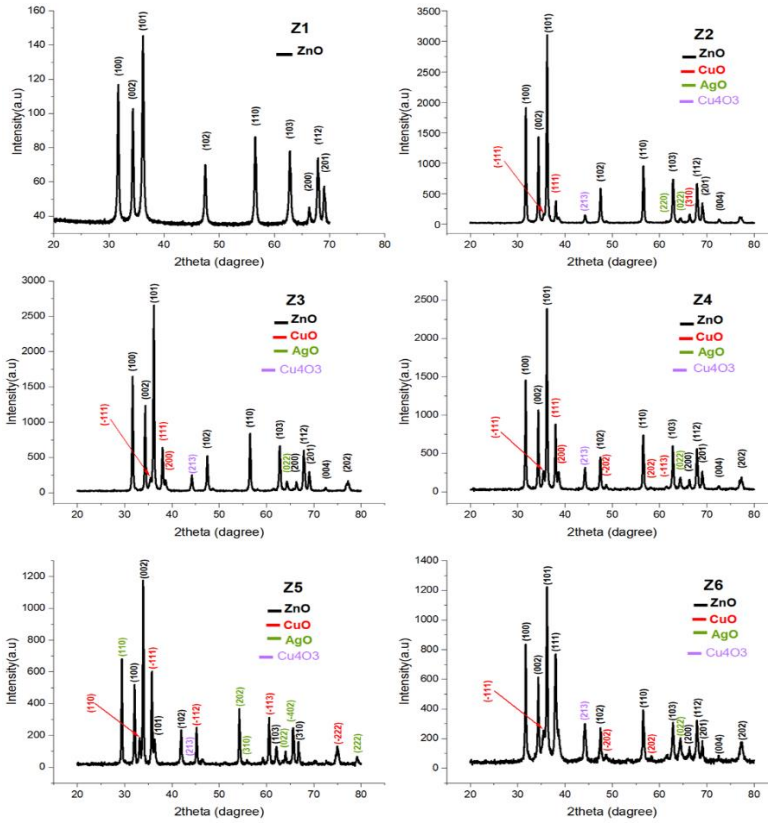

Figure 1. X-ray diffraction pattern of (ZnO) and (ZnO: Cu – Ag) nanoparticles.

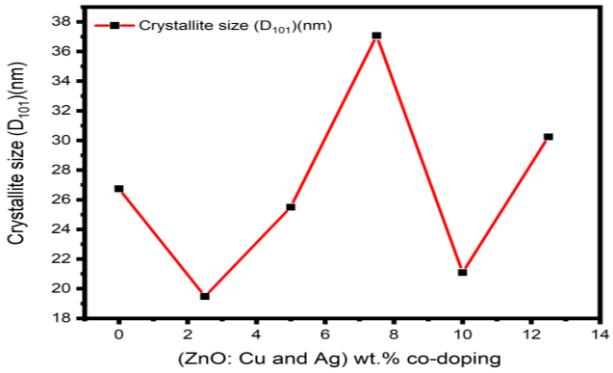

Figure 2. crystal size (D_{101}) as a function of the doping ratios of (ZnO) and (ZnO: Cu - Ag) nanoparticles.

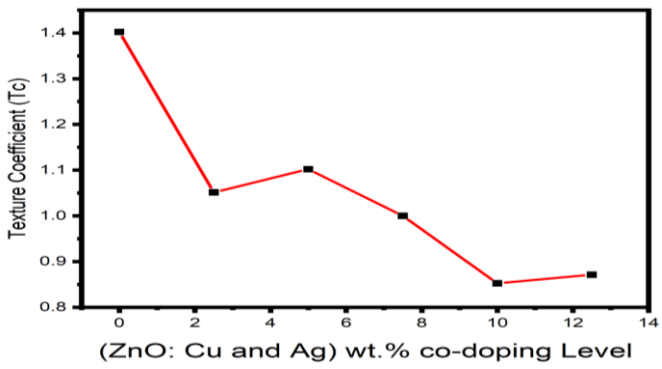

Figure 3. Texture Coefficient (Tc) As a function of the doping ratios of (ZnO) and (ZnO: Cu - Ag) nanoparticles.

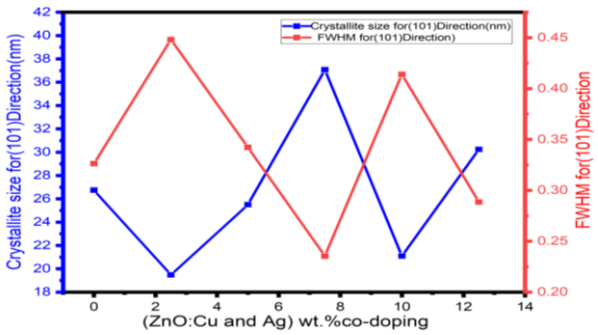

Figure 4. The relationship between (D_{101}) crystal size and (β) full width at half maximum as a function of the doping ratios of (ZnO) and (ZnO: Cu - Ag) nanoparticles.

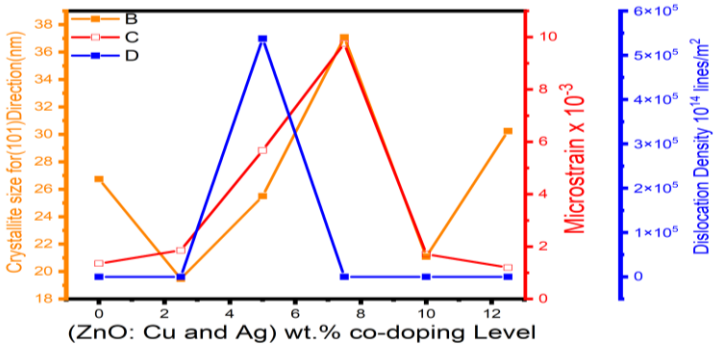

Figure 5. Micro Strain (**ε**), Dislocation Density (**δ**) and crystallite (D101) As a function of the doping ratios of (ZnO) and (ZnO: Cu - Ag) nanoparticles.

Table 2. Diffraction angles, Miller coefficients, full width at half maximum, interfacial distances, and crystallite size.

Sample	2 Theta (degree)	(hkl)	$\mathbf{d_{hkl}}$ (Å)	FWHM (°)	Crystallite size $(\mathbf{D_{hkl}})(\boldsymbol{nm})$
Z1	31.706	100	2.8198	0.419	20.52
	34.392	002	2.6055	0.302	28.70
	36.22	101	2.4778	0.326	26.74
	47.495	102	1.9127	0.418	21.63
	56.57	110	1.625	0.344	27.35
	66.367	200	1.407	0.331	29.91
	67.93	112	1.3788	0.385	25.95
	69.07	201	1.4074	0.384	26.21
Z2	31.75	100	2.815	0.321	26.863
	34.43	002	2.602	0.389	22.297
	36.27	101	1.910	0.441	19.475
	47.55	102	1.624	0.351	25.775
	56.61	110	1.476	0.355	26.4679
	66.36	200	1.407	0.439	22.5289
	67.96	112	1.378	0.402	24.87
	69.09	201	1.358	0.420	23.92
Z3	31.728	100	2.8178	0.38021	22.67
	34.417	002	2.6036	0.47602	18.24
	36.210	101	2.4787	0.34217	25.50
	47.523	102	1.9117	0.4276	21.19

	56.572	110	1.6255	0.39506	23.84
	66.382	200	1.4071	0.42282	23.44
	67.926	112	1.3788	0.41286	24.22
	69.038	201	1.3593	0.4807	20.94
Z4	31.71	100	2.818	0.26354	32.71
	34.381	002	2.606	0.27542	31.52
	36.244	101	2.476	0.2354	37.07
	47.514	102	1.912	0.33066	27.405
	56.574	110	1.625	0.32992	28.54
	66.33	200	1.407	0.40179	24.66
	67.938	112	1.378	0.39552	25.285
	69.07	201	1.358	0.42067	23.935
Z5	66.77578	220	1.3997	0.36288	27.374
Z6	56.58631	110	1.6251	0.3934	23.94
	66.30986	200	1.4084	0.8827	11.22

Table 3. Crystal size (D), Texture Coefficient (Tc), Micro-strain (ε) and Dislocation's density (δ) and full width at half maximum(β).

Sample Code	$\boldsymbol{\beta_{101}}$ (rad)	$\boldsymbol{D_{101}(nm)}$	Tc	$\boldsymbol{\varepsilon \times 10^{-3}}$	$\boldsymbol{\delta \times 10^{-3}}$ $\boldsymbol{(nm)^{-2}}$
Z1	0.3263	26.7439	1.40220	1.35320	1.39813
Z2	0.4481	19.477	1.05142	1.85806	2.635987
Z3	0.34217	25.502	1.10193	1.41907	1.537565
Z4	0.3354	26.019	1	1.39086	1.4770
Z5	0.41393	21.091	0.852401	1.71586	2.47968
Z6	0.28856	30.243	0.871235	1.19663	1.093321

3.1.2 Fourier Transform Infrared Spectroscopy (FTIR) Results

The FTIR spectra of Zinc Oxide Nanobeads (NBs) doped with (Ag-Cu) and undoped samples were collected within the spectral range of 300-4000cm using KBr as a reference. Fourier Transform Infrared Spectroscopy (FTIR) is a highly advantageous analytical technique employed for the examination of materials within the infrared region. This approach facilitates accurate measurements for absorption, transmission, diffusion, as well as emission spectra. The interaction between a sample and infrared light result in inelastic collisions with molecules and infrared photons, leading to the emergence of unique vibrations with discernible frequencies and distinctive patterns, which are contingent upon the exact chemical bond type engaged in the process (A.K. Zak et al.,2011). The samples were subjected to FTIR spectroscopy analysis in order to ascertain the presence of functional groups on metal oxide linkages. Figure 6, illustrates the spectra acquired for both undoped and doped zinc oxide (ZnO) samples. In particular, the absorption band within the range of 3300-3850cm^-1 corresponds to the predictable characteristic expansion of O-H bonds (Mallika AN et al.,2014). The peaks observed within the range

of 1300-1600cm^-1 correspond to the symmetrical and asymmetrical expansion vibrations of C=O, which may potentially be influenced by the presence of KBr due to its tendency to readily absorb CO2. Additionally, the characteristic peak within the range of 360-750 cm^-1 represents modes of metal–oxygen (M–O) (M. Srivastava et al.,2010). Moreover, the stretching mode of ZnO nanostructure appears at 425 cm-1. The broad peak observed in the range 360–660 cm-1 is the combination of Ag-O, Cu–O and Zn–O vibrations (R. Saravanan et al.,2013- Z.S. Li et al.,2006) The introduction of Ag and Cu to the doped ZnO samples results in a decrease in the intensity of this peak, indicating the formation of Ag and Cu clusters on the surface of the ZnO nanoparticles. The displacement of that peak can be ascribed to the modification on the bond length caused by the replacement for Ag+ ions inside the lattice of ZnO positions (A. Modwi et al.,2019)

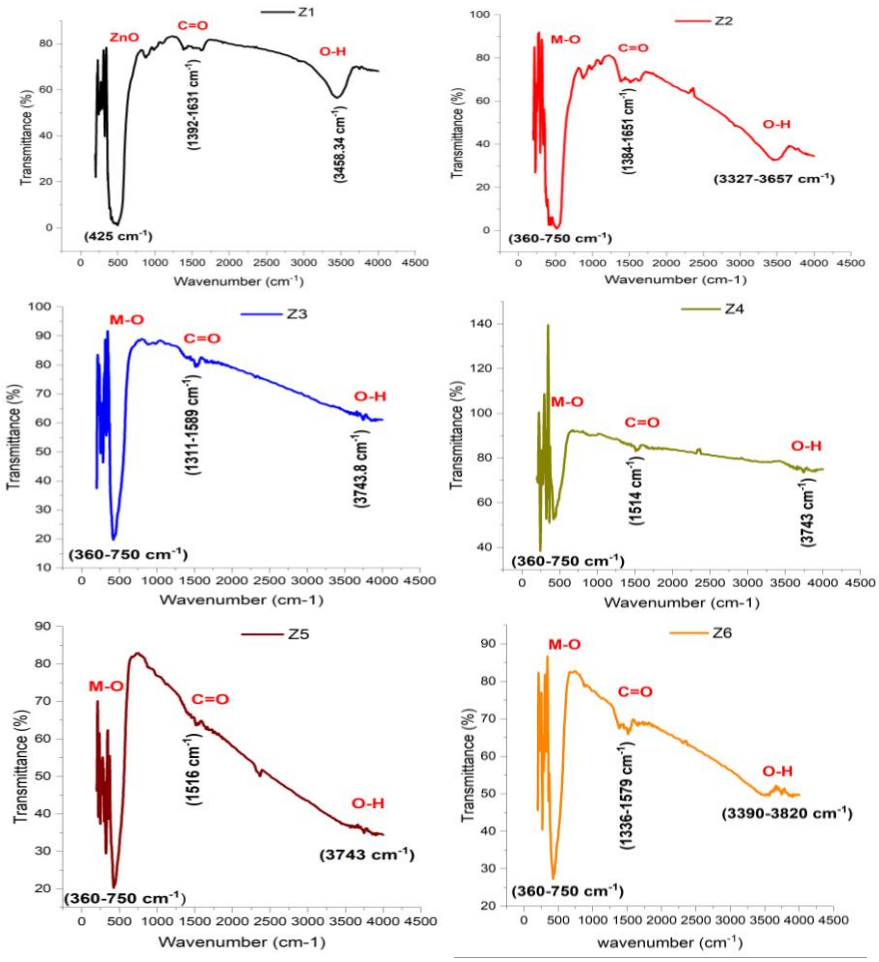

Figure 6. FTIR spectra ZnO and (ZnO: Cu and Ag) of nanoparticles.

3.2 Morphological Properties

3.2.1 Field Emission Scanning Electron Microscopy (FESEM) Result

Due to its ability to magnify and the accuracy of composition, as shown in Figure 7, and at a magnification of 200 nm, The characteristics of the surfaces of (ZnO) nanoparticles were examined using the field-emitting scanning electron microscopy technique. annealed at a constant temperature and doped with silver and copper in different proportions. SEM images revealed nano-sized spherical or quasi-spherical shapes, as the software (Image J) was used for the purpose of calculating the grain size rate, in which the grain diameter (Diameter) was calculated. In order to determine the largest (maximum), average (median), and lowest (minimum), as well as the average particle size (average),

standard deviation, each image has a population rate of between (100-200 granules). Diffraction of X-rays (XRD).

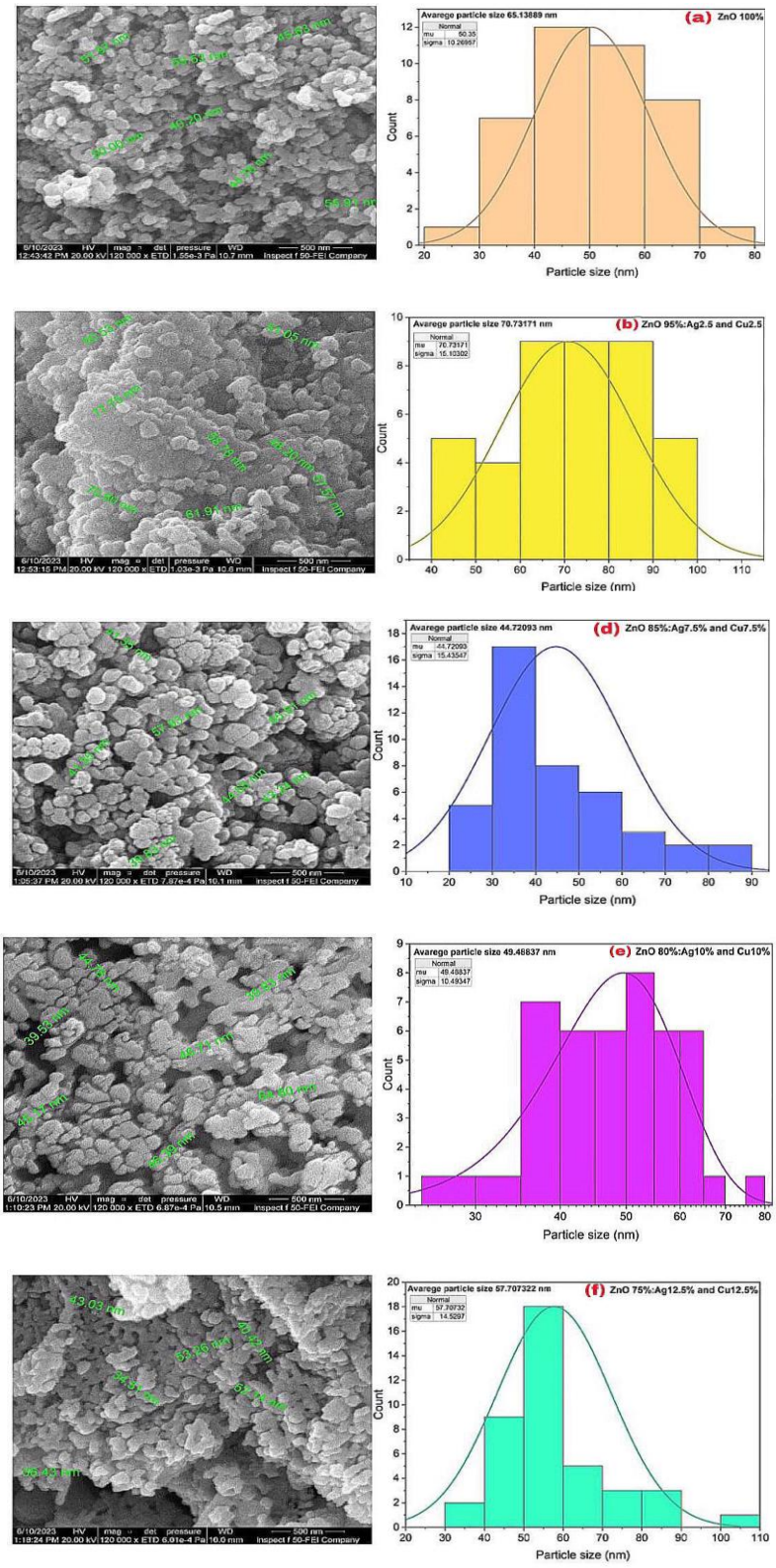

Figure 7. FESEM images of (a- b- c- d- e and f) ZnO and (ZnO: Cu and Ag) of nanoparticles.

Table 4. Standard Deviation and Average Size of FESEM images.

Nanoparticles Types	Standard Deviation	Average Size (nm)
Z1	10.26957	65.13889
Z2	15.10302	70.73171
Z3	14.29652	65.13889
Z4	15.43547	44.72093
Z5	10.49347	49.48837
Z6	14.5297	57.707322

3.2.2 X-ray energy dispersal spectroscopy (EDS) Results

Energy dispersive spectroscopy (EDS) analysis of zinc oxide nanoparticles saturated with silver and copper made by sol-gel method in distilled water are shown in Figures 8.1, 8.2, 8.3, 8.4, 8.5 and 8.7, This supported the outcomes of the (EDS) examination of the copper, silver, and zinc samples.

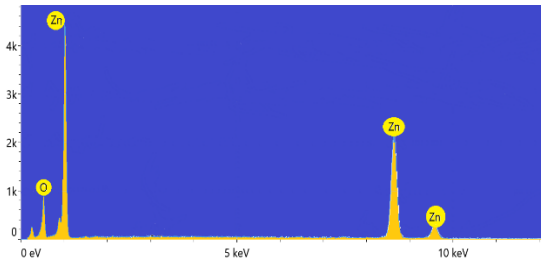

Figure 8.1. EDS spectra analysis of (ZnO 100%).

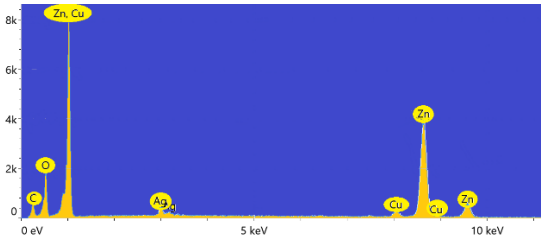

Figure 8.2. EDS spectra analysis of (ZnO 95%: Cu2.5%and Ag2.5%).

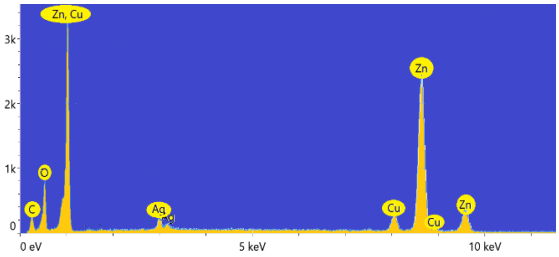

Figure 8.3. EDS spectra analysis of (ZnO 90%: Cu5%and Ag5%).

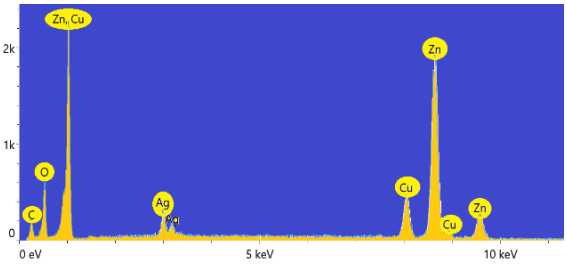

Figure 8.4. EDS spectra analysis of (ZnO 85%: Cu7.5% and Ag7.5%).

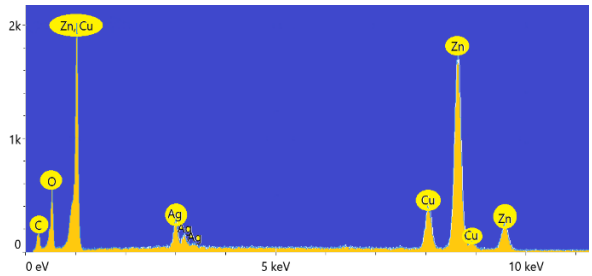

Figure 8.5. EDS spectra analysis of (ZnO 80%: Cu10%and Ag10%).

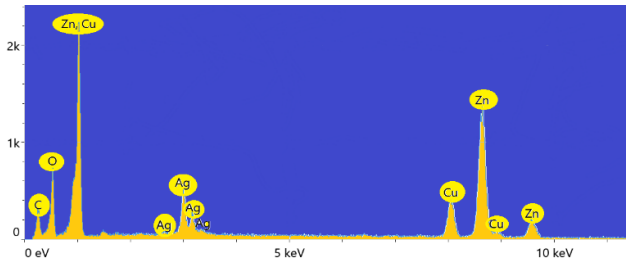

Figure 8.6. EDS spectra analysis of (ZnO 75%: Cu12.5% and Ag12.5%).

Table 5. percentage of ZnO and (ZnO: Cu - Ag) nanoparticles.

Sample	Element	Wt%	Atomic%
Z1	Zn	66.9	31.7
	O	25.1	47.5
	C	8.0	20.8
Z2	Zn	58.3	26.7
	Ag	3.9	1.1
	Cu	2.9	1.4
	C	9.2	22.8
	O	25.7	48.0
Z3	Zn	60.8	31.5
	Ag	4.6	2.5
	Cu	5.9	3.0
	C	8.6	23.0
	O	20.1	40.0
Z4	Zn	57.0	31.5
	Ag	5.8	3.6
	Cu	9.1	6.7
	C	8.7	17.9
	O	19.4	40.3
Z5	Zn	55.6	28.4
	Ag	6.1	1.9
	Cu	11.0	5.8
	C	9.9	27.6
	O	17.4	36.3
Z6	Zn	43.1	19.7
	Ag	10.4	2.9
	Cu	11.2	5.3
	C	10.6	26.4

	O	24.7	45.7

3.3 Optical Properties Results

3.3.1 Absorbance and Optical energy gap

For ZnO particles inlaid with binary fillers with various weight ratios of silver and copper, absorbances at a wavelength range (300-1100 nm) were computed. Since the relationship between wavelength and photon energy is inverse, Electrons must be moved from valence bands to conduction bands (Savka Janković, et al.,2019). and UV-Vis spectra were taken to examine the optical characteristics of Cu and Ag co-saturated ZnO nanostructures, figure 9, Pure ZnO exhibits a peak on the graph at 370 nm, which turns red at 569 nm. With increasing Ag and Cu concentration, the peaks are monotonically moved to a longer wavelength, and as a result, the nanocomposites exhibit considerable visible absorption. By taking into account the well-known surface plasmon resonance (SPR) phenomenon of Ag NPs, this work shows that Ag-containing nanocomposites absorb visible light (S.P. Lim et al.,2014). This large increase in visual absorption shows that the produced nanocomposites can achieve higher visible catalytic efficacy because when Ag is added, the spectral absorption band of (pure ZnO) expand and the absorption edge changes in the direction of a lengthy wavelength (T. Liu et al.,2017).

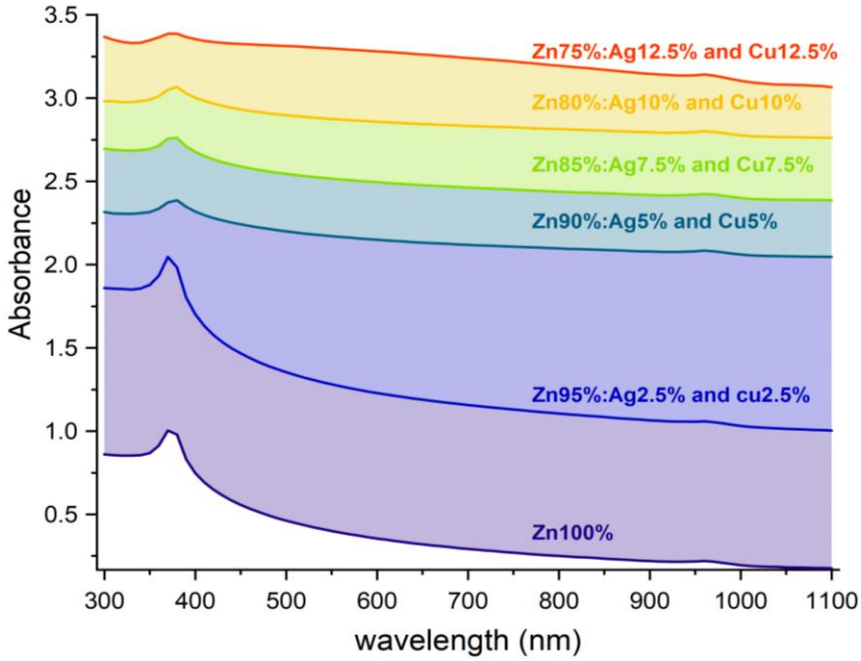

Figure 9. UV-Visible absorption spectra of (ZnO) and (ZnO: Cu and Ag) nanoparticle samples.

the direct transmission optical energy gap was estimated for selected nanoscale findings (Z1, Z2, Z3, Z4, Z5 and Z6). According to the gap values produced by using the (original) program to visualize the relationship between (αhυ)2 and (E), the energy gap is significantly affected by the chemical bonds of its structure components, particle size and general changes (Eg) with particle size change.

$$(\alpha h\nu)^{1/n} = A\,(h\nu - Eg) \quad \ldots \quad (6)$$

Whereas ν is the frequency, h is the Planck constant, Eg is the bandgap energy, α is the absorption coefficient, A is the proportionality constant, and n denotes the type of electronic transition for directly allowed transitions [n = 1/2]. As shown in the figure 10, the energy gap value decreases 3,2.958,2.76,2.74,2.69 and2.5 eV for Z1, Z2, Z3, Z4, Z5 and Z6, respectively. It is obvious that the value of net ZnO (3 eV) is significantly lower than that of big size ZnO (3.37 eV). When particles are shrunk

to the nanoscale the band gap often narrows due to the quantum confinement effect. Additionally, the production of Ag-decorated CuO-ZnO nanoparticles or the partial replacement of Cu and Ag ions inside the ZnO host structure by conquest Zn sites can both have a significant impact on the dwindling in band gap energy with Ag-Cu co-dopings. When compared to pure ZnO, nanocomposites reflect absorption from the Ultraviolet rays to the visible precinct more scatteringly, indicating a potential for their use in visible light-induced photolysis (Z. Han et al.,2012- S. Wang et al.,2014).

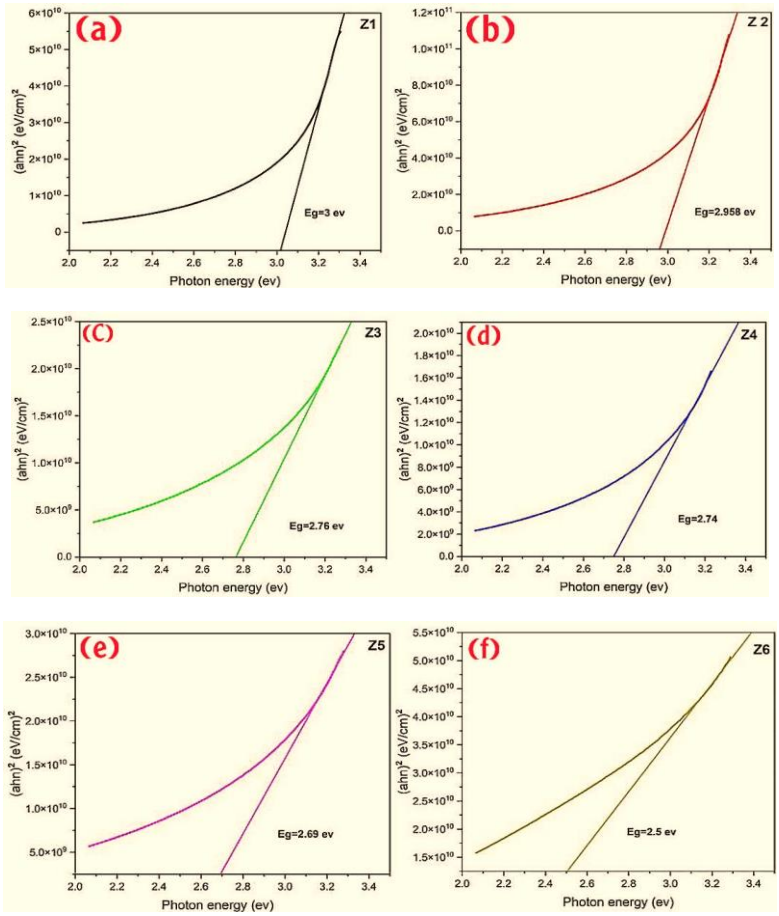

Figure 10. Direct band gap estimations of (ZnO) and (ZnO: Cu and Ag) nanoparticles samples.

4. CONCLUSION

We have successfully prepared ZnO doped with silver and copper using the Sol-Gel method with different weight ratios.

1- XRD spectra confirmed the formation of silver and copper hexagonal ZnO NPs.
2- It was discovered that raising the silver and copper doping ratio results in larger crystals.
3- The acquisition of spherical or nearly spherical nanoparticles is confirmed by the SEM results.
4- The FTIR spectra also confirmed the purity of the silver- and copper-doped ZnO NPS.
5- UV-Visible Spectra - Redshift in absorption spectra due to growing particle size and alteration of morphologies with increasing doping percentages of silver and copper.
6- Zinc, silver, and copper are present, according to EDS information.

REFERENCES

Al Abdullah, K., Awad, S., Zaraket, J., & Salame, C. (2017). Synthesis of ZnO nanopowders by using sol-gel and studying their structural and electrical properties at different temperature. *Energy Procedia*, *119*, 565-570.

Galstyan, V., Comini, E., Baratto, C., Faglia, G., & Sberveglieri, G. (2015). Nanostructured ZnO chemical gas sensors. *Ceramics International*, *41*(10), 14239-14244.

Gnanaprakasam, A., Sivakumar, V. M., & Thirumarimurugan, M. (2016). A study on Cu and Ag doped ZnO nanoparticles for the photocatalytic degradation of brilliant green dye: synthesis and characterization. *Water Science and Technology*, *74*(6), 1426-1435.

Han, Z., Ren, L., Cui, Z., Chen, C., Pan, H., & Chen, J. (2012). Ag/ZnO flower heterostructures as a visible-light driven photocatalyst via surface plasmon resonance. *Applied Catalysis B: Environmental*, *126*, 298-305.

Huang, M. H., Mao, S., Feick, H., Yan, H., Wu, Y., Kind, H., ... & Yang, P. (2001). Room-temperature ultraviolet nanowire nanolasers. *science*, *292*(5523), 1897-1899.

Janković, S., Milisavić, D., Okolić, T., & Jelić, D. (2019). SYNTHESIS OF ZnO-Ag NANOPARTICLES BY SOL-GEL METHOD. *CONTEMPORARY MATERIALS*, *10*(1).

Jorio, A., & Dresselhaus, G. (2008). Carbon nanotubes: advanced topics in the synthesis, structure, properties and applications (Vol. 111). M. S. Dresselhaus (Ed.). Berlin: springer.

Karunakaran, C., Rajeswari, V., & Gomathisankar, P. (2011). Combustion synthesis of ZnO and Ag-doped ZnO and their bactericidal and photocatalytic activities. *Superlattices and Microstructures*, *50*(3), 234-241.

Kołodziejczak-Radzimska, A., & Jesionowski, T. (2014). Zinc oxide—from synthesis to application: a review. *Materials*, *7*(4), 2833-2881.

Kvítek, O., Siegel, J., Hnatowicz, V., & Švorčík, V. (2013). Noble metal nanostructures influence of structure and environment on their optical properties. *Journal of Nanomaterials*, *2013*, 111-111.

Li, Z., Yu, T., Zou, Z., & Ye, J. (2006). Degradation in photocatalytic activity induced by hydrogen-related defects in nano-LiNbO3 material. *Applied physics letters*, *88*(7).

Lim, S. P., Pandikumar, A., Huang, N. M., & Lim, H. N. (2014). Enhanced photovoltaic performance of silver@ titania plasmonic photoanode in dye-sensitized solar cells. *Rsc Advances*, *4*(72), 38111-38118.

Lin, Q., Pearson, R. A., & Hedrick, J. C. (Eds.). (2004). *Polymers for microelectronics and nanoelectronics*. American Chemical Society.

Liu, T., Liu, B., Yang, L., Ma, X., Li, H., Yin, S., ... & Wang, Y. (2017). RGO/Ag2S/TiO2 ternary heterojunctions with highly enhanced UV-NIR photocatalytic activity and stability. *Applied Catalysis B: Environmental*, *204*, 593-601.

Mallika, A. N., RamachandraReddy, A., SowriBabu, K., & Reddy, K. V. (2014). Synthesis and optical characterization of aluminum doped ZnO nanoparticles. *Ceramics International*, *40*(8), 12171-12177.

Meyers, M. A., Mishra, A., & Benson, D. J. (2006). Mechanical properties of nanocrystalline materials. Progress in materials science, 51(4), 427-556.

Modwi, A., Taha, K. K., Khezami, L., Bououdina, M., & Houas, A. (2019). Silver decorated Cu/ZnO photocomposite: efficient green degradation of malachite. *Journal of Materials Science: Materials in Electronics*, *30*, 3629-3638.

Muruganantham, G., Ravichandran, K., Saravanakumar, K., Swaminathan, K., Begum, N. J., & Sakthivel, B. (2012). Effect of solvent volume on the physical properties of sprayed fluorine-doped zinc oxide thin films. *Crystal Research and Technology*, *47*(4), 429-436.

Ravichandran, K., Nithiyadevi, K., Gobalakrishnan, S., Ganapathi Raman, R., Baneto, M., Swaminathan, K., & Sakthivel, B. (2016). Enhancement of photocatalytic efficiency of ZnO nanopowders through Ag+ graphene addition. *Materials Technology*, *31*(14), 865-871.

Samavati, A., Ismail, A. F., Nur, H., Othaman, Z., & Mustafa, M. K. (2016). Spectral features and antibacterial properties of Cu-doped ZnO nanoparticles prepared by sol-gel method. *Chinese Physics B*, *25*(7), 077803.

Saravanan, R., Karthikeyan, S., Gupta, V. K., Sekaran, G., Narayanan, V., & Stephen, A. J. M. S. (2013). Enhanced photocatalytic activity of ZnO/CuO nanocomposite for the degradation of textile dye on visible light illumination. *Materials Science and Engineering: C*, *33*(1), 91-98.

Seyedi, M., Haratian, S., & Khaki, J. V. (2015). Mechanochemical synthesis of Fe2O3 nanoparticles. *Procedia Materials Science*, *11*, 309-313.

Srivastava, M., Ojha, A. K., Chaubey, S., Sharma, P. K., & Pandey, A. C. (2010). Influence of calcinations temperature on physical properties of the nanocomposites containing spinel and CuO phases. *Journal of alloys and compounds*, *494*(1-2), 275-284.

Sun, F., Qiao, X., Tan, F., Wang, W., & Qiu, X. (2012). One-step microwave synthesis of Ag/ZnO nanocomposites with enhanced photocatalytic performance. *Journal of Materials Science*, *47*, 7262-7268.

Tomaev, V. V., Polishchuk, V. A., & Vartanyan, T. A. (2019, January). Optical density of nanocomposite ZnO films doped with Au, Al, Cu. In *AIP Conference Proceedings* (Vol. 2064, No. 1). AIP Publishing.

Vaiano, V., Matarangolo, M., Murcia, J. J., Rojas, H., Navío, J. A., & Hidalgo, M. C. (2018). Enhanced photocatalytic removal of phenol from aqueous solutions using ZnO modified with Ag. *Applied Catalysis B: Environmental*, *225*, 197-206.

Vo-Dinh, T. (2004). A hyperspectral imaging system for in vivo optical diagnostics. IEEE Engineering in Medicine and Biology Magazine, 23(5), 40-49.

Wang, S., Yu, Y., Zuo, Y., Li, C., Yang, J., & Lu, C. (2012). Synthesis and photocatalysis of hierarchical heteroassemblies of ZnO branched nanorod arrays on Ag core nanowires. *Nanoscale*, *4*(19), 5895-5901.
Zak, A. K., Majid, W. A., Abrishami, M. E., & Yousefi, R. (2011). X-ray analysis of ZnO nanoparticles by Williamson–Hall and size–strain plot methods. *Solid State Sciences*, *13*(1), 251-256.

Zaleska-Medynska, A., Marchelek, M., Diak, M., & Grabowska, E. (2016). Noble metal-based bimetallic nanoparticles: the effect of the structure on the optical, catalytic and photocatalytic properties. *Advances in colloid and interface science*, *229*, 80-107.